Spatially resolved Raman scattering from hot acoustic and optic plasmons

A. S. Bhatti, D. Richards, and H. P. Hughes
Optoelectronics Group, Cavendish Laboratory, Madingley Road, Cambridge, CB3 0HE, United Kingdom

D. A. Ritchie
Semiconductor Physics Group, Cavendish Laboratory, Madingley Road, Cambridge CB3 0HE, United Kingdom

(Received 13 November 1995)

A two-dimensional electron gas drifting under a lateral bias is also heated, and the drift and heating have dramatic effects on its collective plasmon modes. A low-energy feature is observed in polarized Raman scattering in addition to the usual intrasubband plasmon mode, and disperses linearly with in-plane wave vector. Large variations in the Raman intensities and energies of the intrasubband plasmon and the low-energy feature are observed with position along the drift channel, together with variations in the electron temperature and in the integrated photoluminescence intensity. These effects are discussed in terms of a simple model involving a second sheet of electrons near the current injection contact; the low-energy mode is ascribed to an additional acoustic plasmon mode arising from this double-electron sheet geometry.

I. INTRODUCTION

Two-dimensional electron gases (2DEG's) drifting under the influence of an in-plane electric field have attracted much attention because of the physical and technological interest in plasmon instabilities in drifting 2DEG's. These have been shown theoretically to occur for drift velocities ν_d equal to or larger than the 2DEG Fermi velocity,[1,2] although such conditions have been shown to be very difficult to achieve experimentally in GaAs/Al$_x$Ga$_{1-x}$As systems[3,4] in which typically $\nu_F \approx 10^7$ cm s^{-1}. Devices such as radiation sources based on plasmon instabilities have been suggested,[5,6] and recent experimental data on a drifting 2DEG have shown that the heating of a 2DEG by an applied field gives rise to ''hot'' plasmons which can be observed in anti-Stokes Raman scattering,[7] and which can decay to far-infrared radiation in the presence of a grating optical coupler.[8] The potential distribution in the drift channel has also received much attention, and instabilities have been observed in high electric fields due to the formation of high-field domains in the drift channel which travel from source to drain.[9]

Electronic Raman scattering, a powerful experimental technique for the investigation of both collective and single-particle electronic excitations (SPE's) in a 2DEG (e.g., Refs. 10 and 11), has recently been used to characterize electronic devices.[7,12] In the backscattering geometry employed here [Fig. 1(a)], the Raman wave-vector transfer in the plane of the 2DEG can be varied by rotating the sample relative to the incident and scattered light wave vectors, enabling the determination of the energy dispersion of the excitations with wave vector q. The 2DEG plasmon energy disperses as $q^{1/2}$, and the high-energy cutoff for SPE's has a linear dispersion $q\nu_F$.[10] The selection rules for inelastic light scattering from the 2DEG allow plasmons to be observed when the incident and scattered polarizations are parallel (polarized scattering), and spin-density excitations when the polarizations are mutually perpendicular (depolarized scattering).[10] However, Raman scattering from SPE's has been observed experimentally for both configurations.[13]

In Raman spectroscopy, the simultaneous measurement of both Stokes (S) and anti-Stokes (AS) scattering allows the observation of excitations with wave vectors in opposite directions. If the wave-vector transfer determined by the experimental geometry is $\mathbf{Q}$, an excitation of wave vector $\mathbf{q}(=+\mathbf{Q})$ is created and observed in Stokes (S) Raman scattering, while in anti-Stokes (AS) scattering an excitation of wave vector $\mathbf{q}(=-\mathbf{Q})$ is annihilated, and the wave vector of the observed excitation is therefore $-\mathbf{Q}$ [Fig. 1(a)]. So for a 2DEG with the drift velocity ν_d in the scattering plane [Fig. 1(a)], the simultaneous Stokes and anti-Stokes Raman spectra correspond to two different configurations, with the excitation wave vector $\mathbf{q}$ parallel and antiparallel to ν_d.

Furthermore, for plasmon excitations, the ratio of the Stokes and anti-Stokes intensities provides a direct estimate of the electron temperature T_e,[14] which can be compared to that determined by analyzing the high-energy tail of the band-to-band photoluminescence (PL).[15] Note, however, that for a degenerate 2DEG ($T_e \ll T_F$, where T_F is the Fermi temperature) PL involves the radiative recombination of electrons with photoexcited holes and hence strictly gives the characteristic hole temperature T_h, which is assumed to be equal to T_e. The two techniques complement each other,[7] though Raman spectroscopy gives a direct measure of T_e, whereas PL is a complicated process, involving spatially direct and indirect transitions and the nature of the electron and hole distribution functions; the PL intensity also depends on the density of the minority carriers.

The application of an in-plane electric field results in an increase in electron temperature, and shifts the 2D Fermi circle in momentum space, leading to a Doppler shift of the 2DEG plasmon modes: $\omega_p = \omega_{p0} + \mathbf{q}\cdot\nu_d$,[7] where ω_{p0} is the plasmon energy for zero drift velocity given by[16]

$$\omega_{p0}^2 = \frac{N_s e^2}{2\varepsilon\varepsilon_0 m^*} q, \tag{1}$$

where N_s is the areal density of electrons, and the screening effects of the various layers in the sample are accounted for

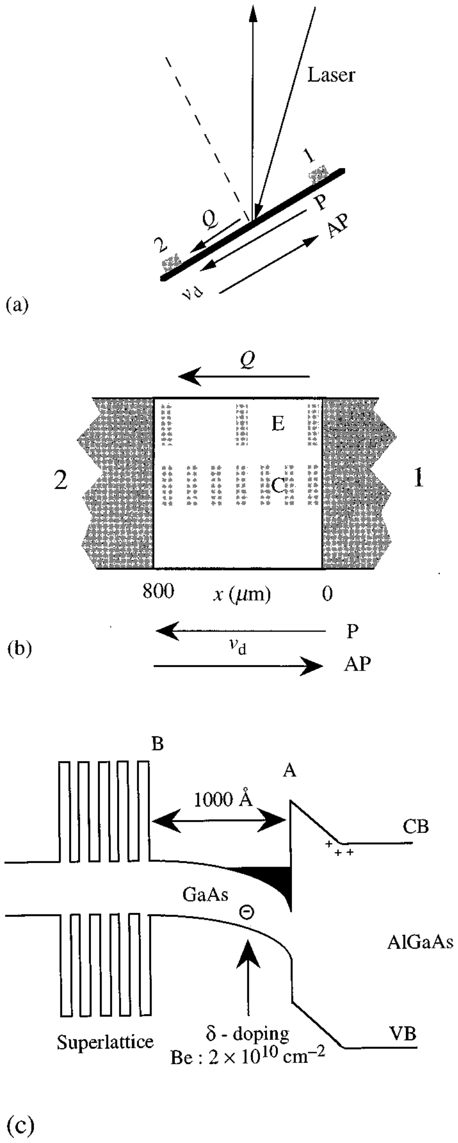

FIG. 1. (a) Backscattering geometry showing the Raman wave-vector transfer Q and the drift velocity v_d [parallel (P) and antiparallel (AP)] to Q as discussed in the text. The in-plane wave vector of the excitations created in Stokes scattering is $q = \pm Q$, and of those annihilated in anti-Stokes scattering is $q = -Q$. 1 and 2 label the two Ohmic contacts for applying the drift bias. (b) Drift channel showing the areas of measurement along the center line (C) and the edge (E) of the mesa etched into the heterojunction sample, and the two directions of v_d, P, and AP to Q. (c) Schematic of the layer structure of the sample, with the GaAs/Al$_x$Ga$_{1-x}$As interface (A) and the GaAs superlattice interface (B).

by the effective dielectric constant ε.[17]

In this paper, the results of spatially resolved Raman and PL measurements from a 2DEG drifting under the influence of a constant in-plane electric field are reported. A number of physical parameters of the system in the drift channel are obtained, such as carrier densities, the magnitude of Doppler shift, and the electron temperature. Furthermore, the spatial resolution allows the study of excitations with position in the drift channel. A large variation in the intensity of the plasmon peak with drift current and position along the drift channel is observed. An additional low-energy feature is also observed in polarized Raman scattering under lateral drift conditions, and may be due to an acoustic plasmon; this feature shifts with current and momentum transfer, and with position along the drift channel. Strong variations in the PL intensity are also observed with position in the drift channel.

II. EXPERIMENT

The sample was a standard GaAs/Al$_{0.3}$Ga$_{0.7}$As-doped heterojunction incorporating a Be δ layer 250 Å from the heterointerface, as shown in Fig. 1(c).[7] The electron mobility and carrier density obtained form Hall measurements at a temperature of 1.6 K were $\mu = (2.2 \pm 0.2) \times 10^5$ cm^2 V^{-1} s^{-1} and $N_s = (2.1 \pm 0.2) \times 10^{11}$ cm^{-2} in the dark, and $\mu = (3.0 \pm 0.3) \times 10^5$ cm^2 V^{-1} s^{-1} and $N_s = (2.5 \pm 0.3) \times 10^{11}$ cm^{-2} after brief illumination by a red light-emitting diode (LED). A mesa-etched area of the sample formed the drift channel of length 800 μm and width 1000 μm, with two primary Au/Ge/Ni Ohmic contacts [contacts 1 and 2, Fig. 1(b)] for applying the in-plane electric field. Raman-scattering experiments were performed using a laser wavelength of 777.5 nm (near resonance with the GaAs E_0 band gap) and for a range of momentum transfers [determined by the backscattering geometry, Fig. 1(a)]. Resonant electronic Raman scattering is thought to be facilitated in this structure by the presence of the ionized Be δ layer which enables hole localization in the vicinity of the 2DEG. The resonance profile for Raman scattering from plasmons was found to be very broad ($\gtrsim 50$ meV). As the Be-doping density is very low (2×10^{10} cm^{-2}, negligible compared to the 2DEG density), the δ layer has a negligible effect on the electrostatic potential.

The laser spot was defocused onto the sample surface with the spot diameter of approximately 1.1 mm covering the whole drift channel, such that the power density (8–10 W cm^{-2}) was approximately uniform over the channel. (Using a laser spot smaller than the drift channel produced a voltage drop across the channel which varied with the position of the spot; however, the Raman results obtained with small and large illumination spots were similar.) The sample image was magnified by a factor of 3 onto an intermediate iris (the diameter is approximately equal to 1000 μm) and the 200-μm-wide entrance slit of the spectrometer, thus probing Raman scattering from an area 70 μm along and 330 μm across the drift channel. Together with the mechanical stability of the sample stage, this led to an overall accuracy of $\sim \pm 50$ μm in the spatial resolution along the drift channel. The lattice temperature was maintained at ~ 7 K on a cold finger in a He bath cryostat. The scattered light was energy dispersed using a DILOR XY triple grating spectrometer and detected with an intensified Si diode array. For zero drift, a peak due to scattering from the 2DEG plasmon was observed in polarized Raman spectra, while no signal was observed for depolarized scattering. Using the 2D plasmon dispersion relation [Eq. (1)], the 2DEG carrier density was estimated under zero drift conditions to be $N_S \approx 3.70 \times 10^{11}$ cm^{-2}.

Drift currents I up to 25 mA, constant to within $\pm 5\%$, were generated by an applied voltage across the end contacts of the drift channel; the current fluctuations arose from variations in the laser power density ($\pm 5\%$). The sample *I*-*V* characteristics were found to be independent of the direction of the lateral biases. The range of drift velocities probed was limited by the associated electron temperature rise, which eventually broadened the band gap PL to higher energies sufficiently to obscure the plasmon Raman peak.

Spatially resolved Raman and PL measurements were made for different positions x [the distance from contact 1 in Fig. 1(b)] along the center (C) (P and AP configurations) and the upper edge (E) (P configuration only) of the drift channel. The source and drain are defined as those contacts from which electrons enter and leave the drift channel, respectively [Fig. 1(b)]. The P (and AP) configurations, i.e., ν_d parallel (and antiparallel) to the Raman wave-vector transfer Q, are achieved when contacts 1 and 2 are used as the source and drain (and vice versa). The bias values ranged up to 1.84 V for the maximum current of 25 mA, corresponding to a lateral field of 23 V cm^{-1}, though most measurements were performed for $I = 15$ mA, for which the plasmon signal was maximum.

III. RESULTS AND DISCUSSION

A. Photoluminescence spectroscopy

Significant changes in the band-gap PL from the drifting 2DEG were observed with position x along the drift channel. The PL spectra showed two distinct peaks due to recombination of degenerate electrons with acceptor bound holes (e-B) and with free holes (e-A).[7,18] Assuming electrons and holes are in thermal equilibrium, the electron temperature T_e is determined by fitting a Boltzmann distribution function to the high-energy tail of the (e-A) PL peak. T_e was also deduced from the ratio of the Stokes and anti-Stokes plasmon Raman intensities (for the drifting 2DEG) at various points in the drift channel. Although a determination of temperature in this way is strictly valid only under nonresonant conditions, when the Raman-scattering amplitudes are independent of the outgoing photon energies, it is justified in this case as the width of the resonance ($\gtrsim 400$ cm^{-1}) is large compared to the energy separation of the Stokes and anti-Stokes peaks (~ 110 cm^{-1}).

T_e for a nondrifting 2DEG (17 ± 1 K) was independent of the position in the drift channel as expected, showing that the illumination density is fairly uniform over the drift channel. Under drift conditions ($I = 15$ mA; lateral electric field 14.2 V cm^{-1}) and concentrating on the line along the center of the drift channel (C), it was found that T_e was lower near the electron source than near the drain; T_e ranged from 29 ± 2 K at the source to 41 ± 2 K at the drain for the P configuration, and from 30 ± 2 K at the source to 43 ± 2 K at the drain for the AP configuration, as shown in Fig. 2(a). T_e determined from Raman measurements along the center of the drift channel in the P configuration are also shown, and the temperatures determined from the two techniques are in good agreement. The change in T_e from source to drain is roughly linear in x. Also shown in Fig. 2(a) are electron temperatures measured close to the upper edge (E) of the drift channel; these are markedly lower than those along the center (C), suggesting that the field near the mesa edge is smaller than at the center.

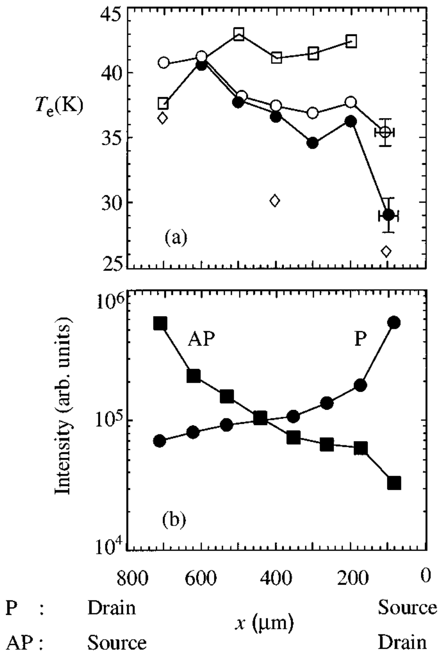

FIG. 2. Variations with position x in the drift channel for (a) the electron temperature T_e along the center C of the channel determined from PL (○,P), (□, AP) and Raman measurements (●,P), and also from PL along the edge E of the channel (◇,P); and (b) the integrated band-gap PL intensities (●,P) and (■, AP).

Figure 2(b) shows the integrated PL intensities for the (e-A) peak as a function of position x along the center of the drift channel for the same conditions as for Fig. 2(a). Large variations are observed, with the PL intensity a maximum close to the source contact and decreasing to a minimum at the drain end. Since the PL process is dominated by the recombination of degenerate electrons with photoexcited valence-band holes, its intensity reflects the density of these minority carriers.

B. Raman spectroscopy

A representative spectrum for polarized Stokes Raman scattering from the nondrifting 2DEG is shown at the bottom of Fig. 3; also shown are polarized Stokes and anti-Stokes Raman spectra for $I = 15$ mA, obtained at various positions x along the drift channel from the source for the case when the drift velocity ν_d is parallel (P) to the Raman wave-vector transfer $Q = 1.25 \times 10^5$ cm^{-1}. The plasmon peak (ω_p) is clearly visible in both Stokes and anti-Stokes spectra, together with a low-energy (LE) feature (ω_X) visible only on the Stokes side.

In Fig. 4, the Raman shifts for the plasmon and the LE feature, ω_p and ω_X, are plotted as a function of x for both the P and AP cases, for $I = 15$ mA; ω_{p0} is also shown and is independent of x, suggesting a uniform 2DEG density in the channel for $I = 0$ mA, and confirming that the channel was illuminated with uniform laser power density. For $\nu_d > 0$, the Stokes and anti-Stokes plasmon energies are a minimum

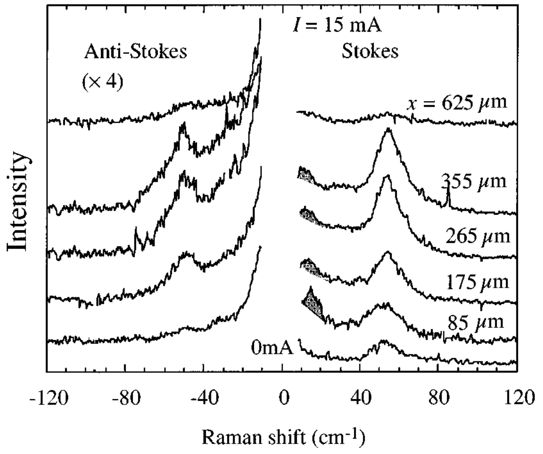

FIG. 3. Stokes (S) and anti-Stokes (AS) polarized Raman spectra for the 2DEG for a drift current $I=15$ mA at various positions x in the drift channel for the P configuration. The source and drain are at $x=0$ and $x=800$ μm, respectively. The Raman wave-vector transfer $Q=1.25\times10^5$ cm^{-1} and the sample temperature is 7 K. The bottom spectrum is for a nondrifting 2DEG. The plasmon peak occurs around ~ 50 cm^{-1}, and the low-energy feature referred to in the text is shown shaded. The spectra are displaced vertically, and the anti-Stokes intensities have been scaled by a factor of 4, for clarity.

close the source, and increase as x increases toward the drain. Assuming a single 2DEG, the average of the Stokes and anti-Stokes Raman shifts gives the non-Doppler-shifted plasmon energy from which the carrier density N_s in the drift channel can be estimated using Eq. (1);[7] for $I=15$ mA, N_s apparently increases by roughly 5% from the source to drain, though this picture is modified in Sec. V.

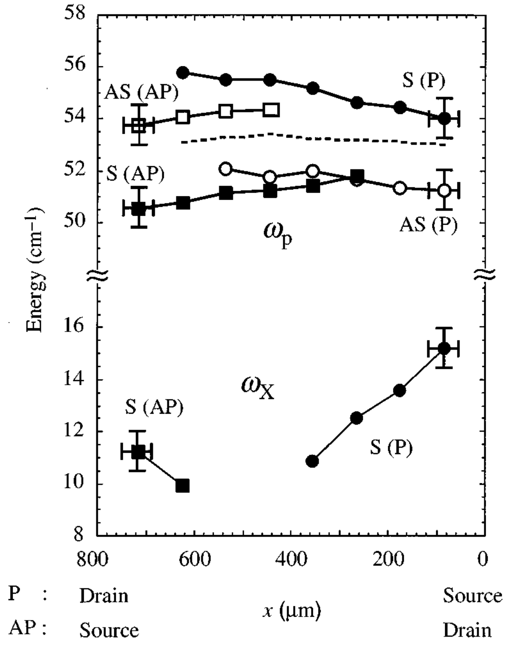

FIG. 4. The energies of the various Raman features for $I=15$ mA as a function of x: Stokes (S) plasmon for P (●) and AP (■) configurations; anti-Stokes (AS) plasmon for P (○) and AP (□) configurations. Stokes low-energy (LE) peak for P (●) and AP (■) configurations. The Stokes plasmon energy for $I=0$ mA is shown as the dashed line.

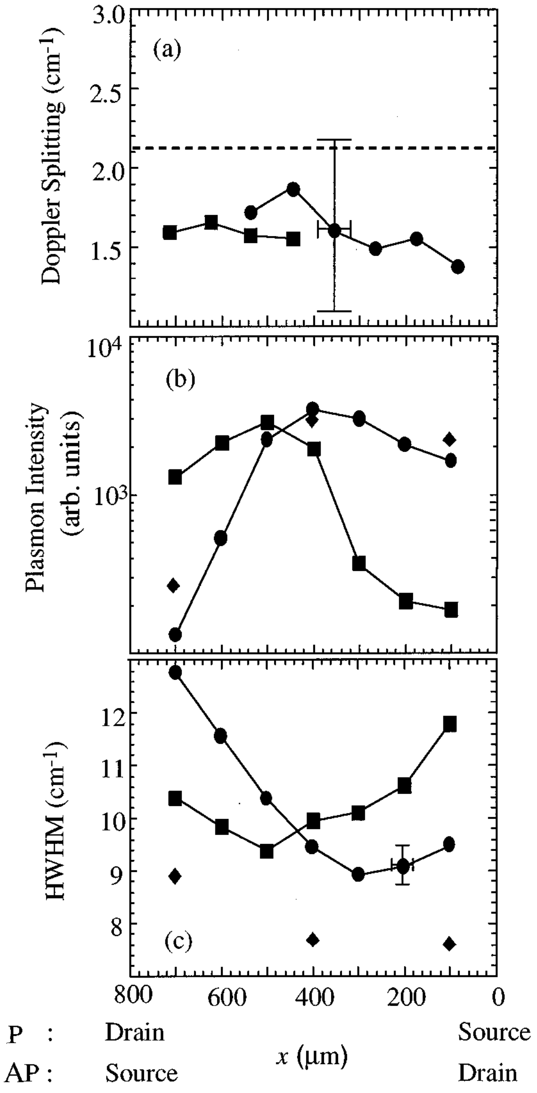

FIG. 5. The variations with position x along the center of the drift channel, for $I=15$ mA and for both the P (●) and AP (■) configurations, of the following: (a) the plasmon Doppler shift. (The dashed line is the predicted shift as discussed in the text.) (b) The plasmon intensity. (c) The plasmon peak width. ◆ correspond to points close to upper edge of the channel for the P configuration.

In Fig. 5(a) the magnitude of the Doppler shift (half the difference between the anti-Stokes and Stokes plasmon energies) is plotted as a function of x; the mean values are $\pm 1.6 \pm 0.6$ cm^{-1} for the P and AP configurations, respectively. The predicted Doppler shift $|q v_d|$ can be estimated, obtaining v_d from $N_s(=4.1\times10^{11}$ cm$^{-2})$ and I, and is also shown. The slight variations with x are within the estimated errors, and may be due to a nonuniform electric field in the drift channel, but there appears to be a significant deviation from $|q v_d|$. The discrepancy between the experimental and theoretical Doppler shifts is at present unexplained, though it has been found that the Doppler shift follows the expected behavior of $\pm q v_d$ only for small v_d, saturating at $v_d > 3.0\times10^6$ cm s^{-1}.[7]

The variation in the Raman plasmon intensities and peak

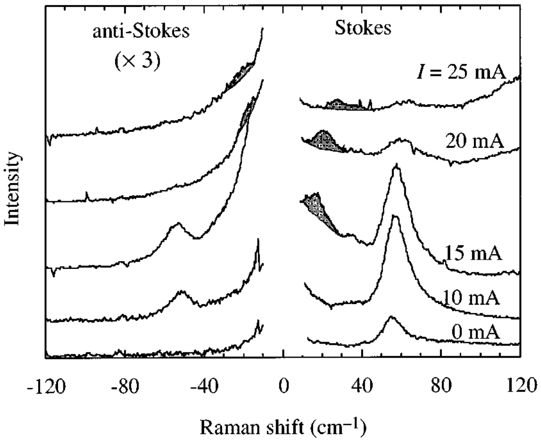

FIG. 6. Stokes and anti-Stokes polarized Raman spectra of the drifting 2DEG with the Raman wave-vector transfer of 1.4×10^5 cm^{-1} parallel (P) to the drift at $x=85$ μm. The plasmon peak occurs around ~50 cm^{-1}, and the LE peaks are shown shaded. The spectra are displaced vertically, and the anti-Stokes intensities have been scaled by a factor of 3, for clarity.

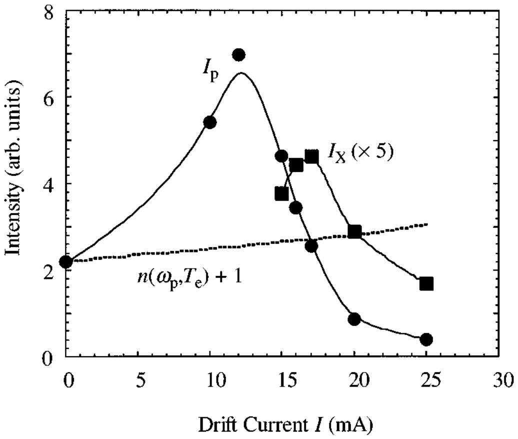

FIG. 7. The intensities I_p and I_X of the Stokes plasmon (●) and the Stokes low-energy model (■) (scaled by a factor of 5) as a function of drift current I for the parallel (P) configuration. The dashed line shows the variation in the plasmon Bose-Einstein factor (arbitrarily normalized at $I=0$ mA) determined from the electron temperatures T_e (ranging from 20 to 65 K) obtained for each value of I from PL.

widths for both P and AP cases as a function of x along the center and the upper edge of the drift channel are plotted in Figs. 5(b) and 5(c), respectively. The behavior for the P and AP configurations are similar. The plasmon intensities increase slightly away from the source and then fall dramatically, with the maximum intensity for both cases occurring at the center of the drift channel where the plasmon intensity is roughly independent of the bias direction; the behavior observed close to the upper edge of the channel follows that along the center of the channel for the P case. This is consistent with the variations for the PL, as Raman scattering is a resonant process depending strongly on the recombination efficiencies of the photoexcited electrons and holes. Recombination efficiencies are known to be affected by the overlap of the electron and hole wave functions and by the carrier densities.

The plasmon peak widths (determined by the electron-scattering times) for both P and AP cases show similar behaviors as a function of position x [Fig. 5(c)], initially decreasing away from the source with a minimum (7% reduction) approximately 300 μm from the source, and subsequently increasing by approximately 40%. The Raman peak widths close to the upper edge are lower than observed along the center of the channel, and again may possibly be due to a nonuniform field distribution in the drift channel. These variations in peak widths cannot be satisfactorily explained at present.

In contrast to the slight *increase* in the plasmon energy ω_p as the sampling point is moved away from the source, there is a drastic *decrease* in the energy ω_X of the low-energy mode (Fig. 4). A possible explanation for this, and the origin of this LE feature, will be discussed in Sec. V.

IV. PLASMON AND LOW-ENERGY MODE

A. Variation with drift current

Stokes and anti-Stokes polarized Raman spectra are shown in Fig. 6 for various drift currents at a fixed position of $x=85$ μm in the drift channel [close to the source (contact 1)], with the wave-vector transfer of 1.4×10^5 cm^{-1} parallel to v_d. As expected, ω_p shifts with I due to the Doppler shift and an increase in the electron density, N_s. T_e rises with I and, as a consequence, the anti-Stokes plasmon peak, corresponding to the annihilation of increasingly numerous ''hot'' plasmons, emerges more strongly.[7] At each value of I, T_e was determined from PL and the Stokes–anti-Stokes intensity ratio (the two techniques agreeing to within ±3 K), and rose form 19 K for 0 mA to 55 K for 20 mA, in good agreement with theoretical predictions.[19]

Figure 7 shows the variation in the observed Stokes intensities of the plasmon and the LE mode as a function of I; the Stokes Raman intensity is expected to follow $n(\omega_p,T_e)+1$, where $n(\omega_p,T_e)$ is the Bose-Einstein occupation number, and this expected variation is also shown, normalized at $I=0$ mA (dotted line). It is clear that the observed Raman intensities cannot be discussed in terms of the Bose-Einstein function; the maxima for the plasmon and the LE mode are at different currents, and these marked variations cannot be explained at present.

With increasing current, the scattered intensity close to the laser line on both the Stokes and anti-Stokes sides increases steadily, and eventually the LE feature appears. The shift in its energy ω_X with I suggests that it is due to electronic excitations, and Fig. 8 shows the variation in ω_p (which has been discussed previously[7]) and ω_X with I; the shift in ω_X is much more marked than that for ω_p. It is also evident from Fig. 8 that the Doppler splitting of the Stokes and anti-Stokes plasmon energies is much larger than that of the LE feature. Also plotted in Fig. 8 is the single-particle cutoff qv_F, with v_F determined from the value of N_s obtained from the mean energy of the Stokes and anti-Stokes plasmon peaks; this shows a very small change with current, suggesting that the LE feature is not due to SPE's.

B. Wave-vector dependence

In order to elucidate the nature of the LE feature, Raman spectra were recorded by varying the in-plane wave vector

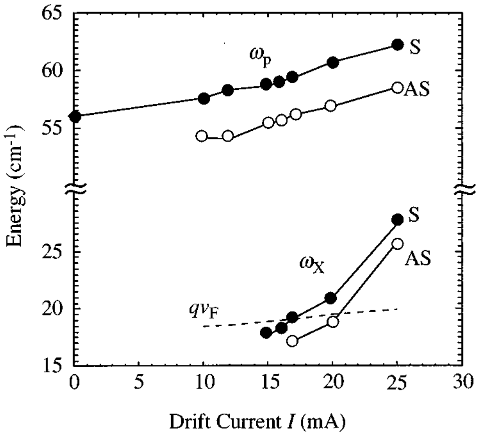

FIG. 8. The energies of the Stokes (●) and anti-Stokes (○) plasmon ω_p and the LE mode ω_X with drift current I at $x = 85$ μm. The dashed line represents the single-particle cutoff qv_F as discussed in the text.

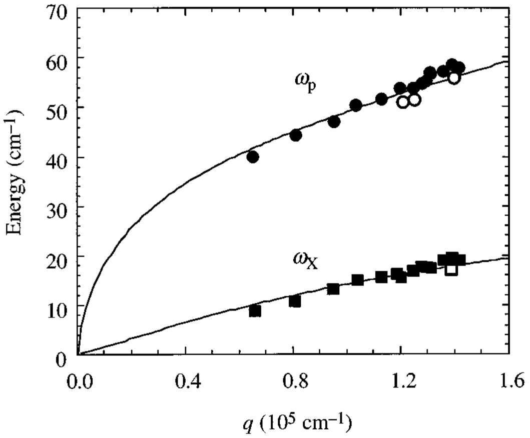

FIG. 10. Dispersion curves of the plasmon (ω_p) and the low-energy feature (ω_X) at $x = 85$ μm for $I = 17$ mA for the P configuration, determined from Stokes (●,■) and anti-Stokes (○,□) spectra. The solid lines are fits based on the double-electron sheet model discussed in the text. The plasmon disperses approximately as $q^{1/2}$, and the low-energy mode approximately linearly with q.

for a fixed drift current of 17 mA (lateral electric field 20.5 V cm^{-1}), and representative spectra are shown in Fig. 9. The experimental dispersions thus obtained are shown in Fig. 10. The linear dispersion of ω_X might suggest that it originates from SPE's, and indeed Raman scattering from intrasubband SPE's of magnitudes comparable to that from the plasmon has been reported in 2DEG systems.[13] The peak of the SPE band should occur close to qv_F, which can be calculated using the 2DEG density N_s obtained from the plasmon dispersion. Although ω_X is close to qv_F here, it shows a much greater variation with I than does qv_F (Fig. 8). It also varies with x; Fig. 11 shows the dispersion of ω_X with wave vector at three different positions in the drift channel for $I = 17$ mA for the P configuration, the solid lines being linear fits through the origin. ω_X is maximum close to the source, and decreases linearly with position in the channel (also see Fig. 4). It should also be noted that no LE signal was observed in depolarized spectra, although Raman scattering from SPE's is expected in this configuration.[13,20] In addition, the sample showed a broad (50 meV) Raman resonance, while SPE's are generally observed only in structures showing sharp resonance behavior.[20] Overall, it appears that SPE's are not the likely explanation for the LE feature, and the observed behavior is discussed in detail in Sec. V, together with possible explanations for the origin of the LE mode.

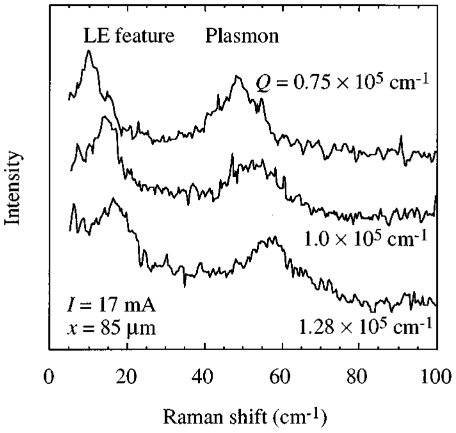

FIG. 9. Representative Stokes polarized Raman spectra for $I = 17$ mA and $x = 85$ μm from the source, for the P configuration for various values of wave-vector transfer Q. The spectra are displaced vertically for clarity.

V. MODEL FOR THE LOW-ENERGY MODE

The linear wave-vector dispersion of the LE mode, once SPE's have been ruled out, suggests a possible explanation as an additional acoustic plasmon mode.[21,22] The emergence of such a mode as a consequence of plasma instabilities in drifting 2DEG's has been predicted to occur for $v_d > v_F$;[1,2,22] however, the maximum drift velocity achieved here is only $0.3v_F$, and the LE mode starts to appear for even smaller drift velocities ($v_d \approx 0.1v_F$), so this explanation is unlikely. Acoustic plasmon modes also exist in plasmas

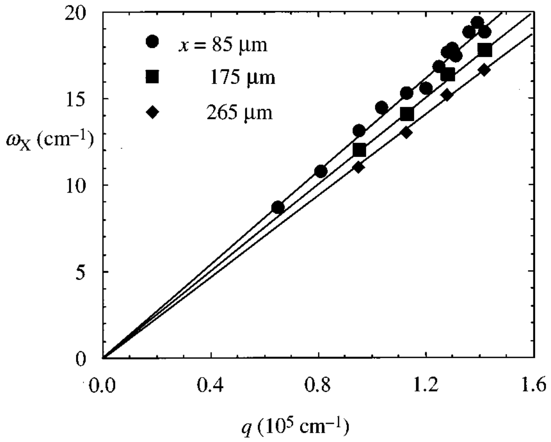

FIG. 11. Dispersion curves for the low-energy feature ω_X at different positions x in the drift channel for a drift current $I = 17$ mA for the P configuration. The solid lines are linear fits passing through the origin.

with two components separated in k space,[22–24] or physically in the sample structure;[21,25] the components oscillating either in or out of phase give rise to optic and acoustic types of behavior. Some possibilities for a second population of electrons here are (i) a second electron population in k space (a hot-electron stream); (ii) occupation of the first excited subband; (iii) an electron gas in the Si-doped $\mathrm{Al}_x\mathrm{Ga}_{1-x}\mathrm{As}$ layer; and (iv) an electron gas confined at interface B [Fig. 1(c)].

There is little likelihood that (i) could be the explanation here, as the LE mode is observed for several hundred μm in the drift channel, while the ballistic scattering length is of the order of a few μm. As regards (ii), the plasmon behavior predicted by random-phase approximation (RPA) calculations of the dielectric response function for this sample[26] show the acoustic mode resulting from occupation of the first excited subband to be very weak in intensity and damped all the time in the electron-hole continuum. This behavior is contrary to the experimental observation. The LE feature is also observed several hundred micrometers away from the source, and the survival of a second subband population injected at the source over such distances would imply an intersubband scattering time unrealistically long compared with those of ($\tau_{01} \approx 100$–200 ps) given by many authors[27] (i.e., $x \approx 200$ μm and $\nu_d \approx 3\times10^6$ cm s^{-1} implies $\tau_{01} \approx 7$ ns). Thus population of the second subband also does not seem likely.

A second electron gas lying parallel to the principal 2DEG would allow modes for which the two spatially separated gases oscillate essentially in phase, producing a combined optic plasmon; or essentially out of phase, producing the lower-frequency acoustic mode with linear wave-vector dispersion. For such a double 2DEG configuration with areal densities N_A and N_B, the dispersion relations for the optic and acoustic plasmon modes are, for $qd \ll 1$ (where d is the separation of the two 2DEG's) and under nondrifting conditions,[21]

$$\omega_{\mathrm{OP}}^2 = \frac{e^2 q}{4\varepsilon\varepsilon_0 m^*}(N_A+N_B)\left(2-\frac{4N_AN_B}{(N_A+N_B)^2}qd\right) \tag{2}$$

and

$$\omega_{\mathrm{AP}}^2 = \frac{e^2 q^2 d}{4\varepsilon\varepsilon_0 m^*}\,\frac{4N_AN_B}{(N_A+N_B)}. \tag{3}$$

However, if the second 2DEG were in the Si-doped $\mathrm{Al}_x\mathrm{Ga}_{1-x}\mathrm{As}$ layer, its mobility would be very low and the associated plasmons would be heavily damped, while the LE feature observed here is quite sharp, with a width approximately half that of the plasmon peak itself.

This leaves the fourth possibility of a second electron gas at interface B, 1000 Å away from the primary 2DEG at interface A [Fig. 1(c)]; such a secondary population might be introduced near the source contact as a result of the injection properties of the nominally Ohmic contact. The solid lines in Fig. 10 are fits to the experimental data using Eqs. (2) and (3) (and therefore neglecting drift) and give $N_A = 3.9\times10^{11}$ cm^{-2} and $N_B = 0.7\times10^{11}$ cm^{-2}, a total areal density of electrons of $N_T = 4.6\times10^{11}$ cm^{-2} as compared with $N_T = 4.1\times10^{11}$ cm^{-2} obtained earlier by fitting the data with a single 2DEG. The inclusion of drift in the calculation of the coupled plasmon modes for a double 2DEG is a complex issue, since different drift velocities are involved because of the different 2DEG mobilities, and has not been attempted here. However, the calculated dispersions for ω_{OP} and ω_{AP} of the optic and acoustic plasmons are in good agreement with those observed experimentally for the plasmon and the LE mode.

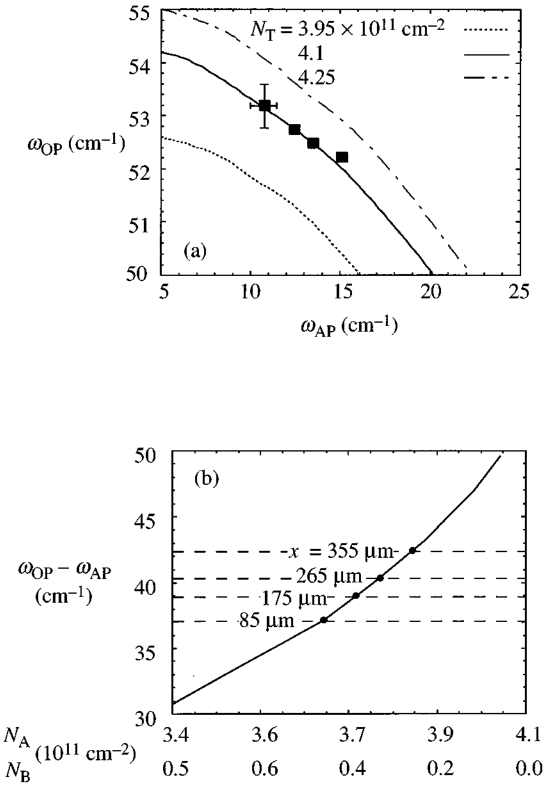

FIG. 12. (a) The optic plasmon energy ω_{OP} vs acoustic plasmon energy ω_{AP}, calculated from the dielectric response of the two-sheet model (see text), varying the areal densities N_A and N_B for three total electron densities $N_T = N_A + N_B$. The adjusted experimental values for several values of x (Fig. 4; see text) are also shown (■). (b) The solid line shows $\omega_{\mathrm{OP}} - \omega_{\mathrm{AP}}$ vs N_A and N_B calculated for a total carrier density $N_T = 4.1\times10^{11}$ cm^{-2}. The horizontal dashed lines mark the experimental values of $\omega_{\mathrm{OP}} - \omega_{\mathrm{AP}}$ for several values of x [see (a)], allowing an estimate of N_A and N_B at these positions.

Further RPA dielectric response function calculations of ω_{OP} and ω_{AP} for two parallel nondrifting 2DEG's, varying N_A and N_B such that N_T remained fixed, are shown in Fig. 12(a), where ω_{OP} is plotted against ω_{AP} for several values of N_T. Also plotted are the experimental values of the energies ω_p and ω_X of the intrasubband plasmon and the LE mode at various positions x along the drift channel ($I = 15$ mA); for comparison with the calculation for nondrifting 2DEG's, ω_p and ω_X have been shifted from the observed Stokes energies by the experimentally determined Doppler shifts of $+1.6$ and $+1.0$ cm^{-1}, respectively. This rough approximation is expected to be valid as the Doppler shift of ω_p is independent of position in the drift channel [Fig. 5(a)] and of drift current (Fig. 8). The curve for $N_T = 3.95\times10^{11}$ cm^{-2} (as obtained earlier, assuming a single 2DEG [Eq. (1)]) lies below the experimental points, but good agreement between theory and experiments is found for $N_T = 4.1\times10^{11}$ cm^{-2}.

The two electron densities at different positions x along interfaces A and B can now be estimated by plotting calculated values of $\omega_{\mathrm{OP}} - \omega_{\mathrm{AP}}$ vs N_A and N_B as in Fig. 12(b). The horizontal dashed lines show the experimental values of $\omega_p - \omega_X$ for $I = 15$ mA at various positions in the drift channel, corrected for drift as discussed above. The intersections of these lines with the calculated curve give estimates of N_A and N_B along the drift channel, and it appears that charge is steadily transferred from interface A to B as the observation point moves away from the source contact. So, assuming that the total electron density in the drift channel remains constant, the balance of the two densities varying along the drift channel can account for the observed variation in the energy of the LE mode in terms of an acoustic plasmon.

However, although this double 2DEG model predicts mode energies similar to those observed experimentally, it fails to predict the variation in intensity of the two modes with x; the ratio of the observed intensity of the plasmon to that of the LE mode increases away from the source, while the ratio obtained from the RPA dielectric response function calculations is almost constant in the region of interest. But the model does allow a semiquantitative interpretation of the observed LE feature. The LE mode is observed close to the source contact where electrons are injected, and where it is assumed that some proportion are confined as interface B. N_B is a function of the injection current and, because the electrons at B have a finite lifetime, also of position along the drift channel. With increasing current, N_B increases, and the LE feature emerges and its energy ω_X increases (Figs. 6 and 8); as N_B decreases along the drift channel due to migration of electrons to the primary 2DEG at interface A, ω_X also decreases (Figs. 4 and 12), the linear decrease suggesting that N_B also decreases approximately linearly along the drift channel. The corresponding increase in N_A causes the (optic) plasmon energy to increase as observed.

VI. CONCLUSIONS

Spatially resolved Raman and photoluminescence measurements on a 2DEG heterojunction sample under lateral bias have shown that the resulting drift and heating of the 2DEG has dramatic effects on the observed plasmon modes. Hot plasmons were observed in anti-Stokes scattering, and the Stokes–anti-Stokes ratio allows a determination of the electron temperature which is complementary to that from the high-energy tail of the band-gap photoluminescence. The electron temperature was found to vary along the drift channel.

Another mode was observed near the source contact of a 2DEG heterojunction sample under conditions of lateral bias, in addition to the usual intrasubband plasmon. The mode was found to disperse linearly with wave-vector transfer, and a model involving two 2DEG's can explain the existence and behavior of this mode as an acoustic plasmon. The model accounts for the variation in the acoustic plasmon and optic plasmon energies as functions of drift current and position along the drift channel, but cannot quantitatively describe the variations in its Raman intensity.

ACKNOWLEDGMENTS

Thanks are due to Dr. L. C. Ó Súilleabháin for sample design, and to Dr. D. Hasko for technical assistance. A.S.B. thanks the Association of the Commonwealth Universities and the Charles Wallace Pakistan Trust for financial support. D.R. acknowledges the Lloyd's of London Tercentenary Foundation for support. This work was funded by UK EPSRC.

---

[1] J. Chen, K. Kempa, and P. Bakshi, Phys. Rev. B **38**, 10 051 (1988).

[2] P. Bakshi and K. Kempa, Phys. Rev. B **40**, 3430 (1989).

[3] W. Masselink, Semicond. Sci. Technol. **4**, 503 (1989).

[4] L. S. Tan, S. J. Chua, and V. K. Arrora, Phys. Rev. B **47**, 13 868 (1993).

[5] K. Kempa, P. Bakshi, and H. Xie, Phys. Rev. B **48**, 9158 (1993).

[6] M. I. Dyakonov and M. S. Shur, Phys. Rev. Lett. **71**, 2465 (1993).

[7] A. S. Bhatti, D. Richards, H. P. Hughes, D. A. Ritchie, J. E. F. Frost, and G. A. C. Jones, Phys. Rev. B **51**, 2252 (1995).

[8] K. Hirakawa, K. Yamanaka, M. Grayson, and D. C. Tsui, Appl. Phys. Lett. **67**, 2326 (1995).

[9] A. Straw, A. Da Cunha, N. Balkan, and A. J. Vickers, Semicond. Sci. Technol. **9**, 619 (1994).

[10] G. Abstreiter, M. Cardona, and A. Pinczuk, in *Light Scattering in Solids IV*, edited by M. Cardona and G. Guntherodt (Springer, Heidelberg, 1984), p. 5.

[11] A. Pinczuk and G. Abstreiter, in *Light Scattering in Solids V*, edited by M. Cardona and G. Guntherodt (Springer, Heidelberg, 1988), p. 153.

[12] L. C. Ó Súilleabháin, H. P. Hughes, D. Bangert, A. C. Churchill, D. A. Ritchie, M. Grimshaw, and G. A. C. Jones, Phys. Rev. B **50**, 14 161 (1994).

[13] D. Richards, B. Jusserand, H. Peric, and P. Etienne, Phys. Rev. B **47**, 16 028 (1993).

[14] M. Cardona, in *Light Scattering in Solids II*, edited by M. Cardona and G. Guntherodt (Springer, Heidelberg, 1982), p. 32.

[15] J. Shah and R. C. C. Leite, Phys. Rev. Lett. **22**, 1304 (1969).

[16] F. Stern, Phys. Rev. Lett. **18**, 546 (1967).

[17] E. Batke, D. Heitmann, and C. W. Tu, Phys. Rev. B **34**, 6951 (1986).

[18] I. V. Kukushkin, K. von Klitzing, K. Ploog, and V. B. Timofeev, Phys. Rev. B **40**, 7788 (1989).

[19] X. F. Wang and X. L. Lei, J. Phys. Condens. Matter **6**, 5667 (1994).

[20] B. Jusserand, D. R. Richards, G. Fasol, G. Weimann, and W. Schlapp, Surf. Sci. **229**, 394 (1990).

[21] S. Das Sarma and A. Madhukar, Phys. Rev. B **23**, 805 (1981).

[22] K. Kempa, P. Bakshi, J. Cen, and H. Xie, Phys. Rev. B **43**, 9273 (1991).

[23] K. el Sayyed, R. Binder, D. C. Scott, and S. W. Koch, Phys. Rev. B **47**, 10 210 (1993).

[24] D. C. Scott, R. Binder, M. Bonitz, and S. W. Koch, Phys. Rev. B **49**, 2174 (1994).

[25] G. E. Santoro and G. F. Giuliani, Phys. Rev. B **37**, 937 (1988).

[26] G. Fasol, R. D. King-Smith, D. Richards, U. Ekenberg, N. Mestres, and K. Ploog, Phys. Rev. B **39**, 12 695 (1989).

[27] R. A. Höpfel, R. A. Rodrigues, Y. Iimura, T. Yasui, Y. Segawa, Y. Aoyagi, and S. M. Goodnick, Phys. Rev. B **47**, 10 943 (1993).